Influence of the linear Stark effect on electron capture into fully stripped ions

Joachim Burgdörfer
Institut für Atom und Festkörperphysik, Freie Universität Berlin, Boltzmannstrasse 20, 1000 Berlin 33, Germany
(Received 10 April 1981)

The complete density matrix for electron capture into the hydrogenic $n = 2$ projectile level is calculated within a modified Oppenheimer-Brinkmann-Kramers approximation which analytically takes into account the long-range coupling effects between the degenerate states of the projectile. The incorporation of the post-collisional Stark effect removes the shortcoming of the first-order calculations of relative l cross sections and of the alignment. We find reasonable agreement between the calculated s-p coherence and the data of Sellin *et al*. The experimentally observed shift of the coherent signal can be explained by the transient inhomogeneity of the external electric field.

I. INTRODUCTION

During the last few years a large number of experimental attempts have been undertaken to get more detailed information on the electron-capture process in energetic ion-atom collisions. As is well known, the total capture cross section σ provides little information on the collision dynamics because an average over all scattering angles and over all substates centered at the projectile is measured. More direct information can be obtained from measurements of substate cross sections,[1-6] differential cross sections,[7-9] and Zeeman coherences[10-12] by atom-photon coincidence measurements. In hydrogenlike projectiles coherences between different orbital-angular momentum states can also be observed because of the quasidegeneracy. Sellin *et al*.[13] first observed the s-p coherence in $n = 2$ hydrogen after electron capture from helium. Dehaes and Singer[14] have recently reported on s-d coherences in $n = 4$ for various targets.

Total cross sections are dominated in the medium-to-high energy range by the low-lying s states. As is well known, the simplest first-order theory, the Oppenheimer-Brinkmann-Kramers (OBK) approximation,[15] largely overestimates the absolute cross section. A reduction can be achieved within various schemes like the "full" Born (B1) approximation (including the internuclear potential),[16,17] the nonorthogonality correction,[18] or the Glauber phase approximation.[19-21] Also various second-order theories, the second-order Born (B2) approximation,[22,23] the impulse approximation (IA),[24] the continuum-distorted wave (CDW) method,[25] and the continuum-intermediate states (CIS) approximation[26] lead to lower cross sections and to better agreement with the experiment.

The situation becomes very different for the angular momentum distribution of the captured electron. Various approximations discussed so far show close agreement with the OBK approximation for relative cross sections of capture into different l states even though the absolute magnitude deviates strongly. For capture into excited states this fact yields the well-known scaling rules[21,27,28] which hold not only for first-order theories like the B1 or the Glauber approximation, but even for second-order theories like the CIS.[29] However, for capture into hydrogenic states, the predicted relative cross sections show a large discrepancy compared with the experiments,[5,29] and also with extensive coupled-states calculations,[18,30-37] which may be regarded as the most reliable theoretical treatment in the considered energy range ($v \gtrsim v_0 = e^2/\hbar$). A common feature is an overestimate of the $l \neq 0$ cross sections compared with the corresponding s cross section of the same principal shell. This shortcoming is also of crucial importance for our present investigation of coherences in the $n = 2$ density matrix.

In the following we shall show that the first-order approximation of the relative l cross section for charge transfer into the $n = 2$ level of a hydrogenic projectile fails, since it neglects the Stark mixing between the degenerate excited states of the projectile escaping the field of the residual target ion. The coupling between states of the same principal shell long after the primary charge transfer has taken place will hereafter be named the "post-collision interaction" (PCI). Obviously, this mechanism is implicitly contained in the numerical coupled-states calculation provided a sufficiently large basis set and interval of time integration is chosen.[33-35] Its importance can be demonstrated within a very simple, analytically soluble model (Sec. II). Applying the PCI model to the OBK approximation for the primary capture process, we find improved agreement of the relative l cross section and the alignment parameter with numerical results and experimental data (Sec. III). As an additional phase-sensitive test for the model, a detailed comparison with the s-p coherence data of Sellin *et al*.[13] is given (Sec. IV). First results on capture-induced s-p coherence have been reported earlier.[38] In the

present extended treatment, the influence of the delayed switch-on of the external electric field on the quantum beat pattern is also investigated. It can explain the experimentally observed shift in the coherent part of the Lyα signal. The analysis enables a more detailed test for the calculated phase and degree of s-p coherence. Some concluding remarks will be given in Sec. V. Explicit expressions for the OBK density matrix for arbitrary n and for the time-resolved Lyα intensity in an external electric field after coherent excitation can be found in appendices A and B, respectively.

II. THE POST-COLLISION INTERACTION MODEL

We consider a charge transfer between hydrogenic orbitals ψ_{1s} and ψ_{2lm} around the target and the projectile with energies $\epsilon_{T,P}$ and charges $Z_{T,P}$. Using the impact-parameter method and choosing the projectile velocity v parallel to the z (quantization) axis, the electron capture amplitude at the projectile position

$$\vec{R}=\vec{b}+\vec{v}t \tag{1}$$

is given in the OBK approximation by

$$a_{2lm}^{\mathrm{OBK}}(\vec{b},Z)=-\frac{i}{\hbar}\int_{-\infty}^{Z/v}dt\exp\left[\frac{it}{\hbar}\left(\epsilon_P+\frac{mv^2}{2}-\epsilon_T\right)\right]\times\int d\vec{r}\,\psi_{2lm}^{*}(\vec{r}-\vec{R})\left(\frac{-Z_T e^2}{r}\right)\times\psi_{1s}(\vec{r})\exp\left(-\frac{\mathrm{Im}\,\vec{v}\cdot\vec{r}}{\hbar}\right). \tag{2}$$

In (1) $\vec{b}$ denotes the vectorial impact parameter and $Z=vt$. The OBK approximation and any other first-order treatment contain only a short-range coupling between the initial and the final state and no coupling of intermediate states. The range is given by the overlap between the target and the projectile wave function and is of the order of the excited state radius $R_0=\langle r\rangle_{n=2}$. However, the coupling between different projectile states due to the electron-target interaction

$$H_{nlm,n'l'm'}=\left\langle nlm\left|\frac{-Z_T e^2}{|\vec{r}'+\vec{R}(t)|}\right|n'l'm'\right\rangle, \tag{3}$$

where $\vec{r}'$ denotes the electron coordinates with respect to the projectile, remains important at much larger distances. This post-collision interaction can be approximated by neglecting small couplings to other principal shells and by using the fact that the spin independence of the high-energy capture amplitude (2) remains valid in the region where the target field is still effective. The evolution in the PCI region ($Z\gtrsim Z_0$) is thus governed by the Hamiltonian (3) and can be described for the $n=2$ level by

$$a_{lm}^{\mathrm{PCI}}(\vec{b},Z,Z_0)=\sum_{l',m'}U_{lm,l'm'}^{\mathrm{PCI}}(\vec{b},Z,Z_0)a_{l'm'}^{\mathrm{OBK}}(\vec{b},Z_0). \tag{4}$$

The starting point of the PCI is denoted by Z_0, which can depend on the impact parameter b. In the OBK amplitude (2) Z_0 entering in the upper limit of the time integration can be pushed to infinity because of exponential damping at large distances:

$$a^{\mathrm{OBK}}(\vec{b})=\lim_{Z_0\to\infty}a^{\mathrm{OBK}}(\vec{b},Z_0), \tag{5}$$

i.e., the usual asymptotic OBK amplitudes can be used in (4).

In the following we shall derive an analytical approximation of the evolution operator (4). A check of this approximation by a comparison with a numerical calculation of the PCI evolution will be given in Sec. III.

Since the main contributions to the OBK amplitude stem from small impact parameters, the electric field acting on the captured electron is already nearly parallel to the beam direction when the projectile enters the PCI region at Z_0. Using $b\approx 0$ and $Z\approx R$, one finds, due to the azimuthal symmetry, only one nonvanishing off-diagonal matrix element

$$H_{2s,2p_0}(Z)=Z_T e^2\left[\exp\left(\frac{-Z}{a_P}\right)\left(\frac{1}{8}\frac{Z^2}{a_P^3}+\frac{1}{2}\frac{Z}{a_P^2}+\frac{3}{2a_P}+\frac{3}{Z}+\frac{3a_P}{Z^2}\right)-\frac{3a_P}{Z^2}\right], \tag{6}$$

with $a_P=a_0/Z_P$ the effective Bohr radius of the projectile. In a multipole expansion of the Coulomb interaction the leading Coulomb term proportional to R^{-1} in the diagonal elements becomes state-independent at large distances and can be removed by a phase transformation. Consequently, the dipolar coupling (6), which decreases as R^{-2}, dominates the evolution because of the faster decay ($\sim R^{-3}$) of the splitting originating from the quadrupolar part of the interaction. Treating the levels as degenerate, the problem is reduced to the time-dependent linear Stark effect. The evolution operator can be obtained analytically, which yields for (4) (apart from a common phase factor):

$$a_{2s}^{\mathrm{PCI}}(\vec{b},Z,Z_0)=\cos\phi\,a_{2s}^{\mathrm{OBK}}(\vec{b})+i\sin\phi\,a_{2p_0}^{\mathrm{OBK}}(\vec{b}), \tag{7a}$$

$$a_{2p_0}^{\mathrm{PCI}}(\vec{b},Z,Z_0)=\cos\phi\,a_{2p_0}^{\mathrm{OBK}}(\vec{b})+i\sin\phi\,a_{2s}^{\mathrm{OBK}}(\vec{b}), \tag{7b}$$

$$a_{2p_{\pm1}}^{\mathrm{PCI}}(\vec{b},Z,Z_0)=a_{2p_{\pm1}}^{\mathrm{OBK}}(\vec{b}), \tag{7c}$$

with

$$\phi = \frac{-1}{\hbar v}\int_{Z_0}^{Z} H_{2s,2p_0}(Z')\,dZ' . \tag{8}$$

The final PCI capture amplitudes are then given by

$$a^{\mathrm{PCI}}(\vec{b},Z_0) = \lim_{Z\to\infty} a^{\mathrm{PCI}}(\vec{b},Z,Z_0) . \tag{9}$$

In this limit, we find for the evolution phase [Eq. (8)] as a function of the lower bound Z_0

$$\phi(Z_0) = \frac{Z_T v_0}{v}\left\{\frac{3a_P}{Z_0} - \exp\left(\frac{-Z_0}{a_P}\right)\left[\frac{1}{8}\left(\frac{Z_0}{a_P}\right)^2 + \frac{3}{4}\left(\frac{Z_0}{a_P}\right) + \frac{9}{4} + \frac{3a_P}{Z_0}\right]\right\} . \tag{10}$$

For distances larger than $Z_1 \approx 10^3$ a.u. the PCI coupling (6) becomes smaller than the fine structure splitting in hydrogen. In this region the evolution of the density matrix is governed by the internal atomic interactions, the fine structure (FS), the hyperfine structure (HFS), and the Lamb shift (E_L). As usual, the orbital angular amplitudes (9) serve as the initial values of the atomic evolution.[39] For the transition, the condition of a sudden approximation is fulfilled because the passage time Z_1/v is small compared with the internal coupling time $\omega_{\mathrm{FS}}^{-1}$. The choice for the lower bound (Z_0) of (10), which is clearly not uniquely defined, needs some discussion. In the following we set Z_0 equal to the smallest $n=2$ radius:

$$Z_0 = \langle r\rangle_{2p} . \tag{11}$$

This choice is suggested by the basic assumption of the model: a separated treatment of the short-range part of the interaction, where the excited state is formed, and of the long-range part, where the capture amplitude is modified by the field of the target ion. The radius of the excited state seems to be a natural intersection of both regimes. For smaller $Z_0 < \langle r\rangle_{2p}$, couplings to many other projectile and target states become important and the restriction to the subspace (4) would no longer be valid. The choice (11) is also supported by the comparison of the analytical approximation with the numerical calculation of the PCI evolution (4) (see Sec. III). Substituting (11) into (10), we finally get

$$\phi = \frac{Z_T v_0}{v}\left(\frac{3}{5} - \frac{389}{40}e^{-5}\right) . \tag{12}$$

The phase depends only on Z_T, not on Z_P. For high velocities, ϕ tends to zero. Nevertheless, even at asymptotically high velocities, the PCI capture amplitudes deviate from the OBK limit because of the different velocity dependence of the OBK amplitudes a_{2s} and a_{2p_0}. This limit should not be taken too seriously, because at very high energies the first-order approximation (2) ceases to be valid. There, the second-order double-scattering mechanism dominates.[40]

III. THE DENSITY MATRIX

For experiments integrating over the scattering angles, the subensemble of $n=2$ excited projectiles can be described by an (unnormalized) axially symmetric density matrix, which is given within the PCI approximation by

$$\sigma^{\mathrm{PCI}}_{l|m|,l'|m'|} = 2\pi\delta_{mm'}\int_0^\infty db\, b\, a^{\mathrm{PCI}}_{lm}(b)(a^{\mathrm{PCI}}_{l'm'})^*(b) . \tag{13}$$

It possesses rotational symmetry around the beam axis and reflection symmetry with respect to every plane containing the beam axis. The diagonal elements correspond to the substate cross sections $\sigma_{00,00}=\sigma_s$, $\sigma_{10,10}=\sigma_{p0}$ and $\sigma_{p\pm1,p\pm1}=\sigma_{p\pm1}$. The only possible off-diagonal element ($\sigma_{00,10} = \sigma_{sp,L}$) denotes the coherence between the s and the p_0 states, the longitudinal s-p coherence. With the help of (7) we obtain the following explicit expressions of (13):

$$\sigma_s^{\mathrm{PCI}} = \cos^2\phi\,\sigma_s^{\mathrm{OBK}} + 2\sin\phi\cos\phi\,\mathrm{Im}\sigma_{sp,L}^{\mathrm{OBK}} + \sin^2\phi\,\sigma_{p0}^{\mathrm{OBK}} , \tag{14a}$$

$$\sigma_{p0}^{\mathrm{PCI}} = \cos^2\phi\,\sigma_{p0}^{\mathrm{OBK}} - 2\sin\phi\cos\phi\,\mathrm{Im}\sigma_{sp,L}^{\mathrm{OBK}} + \sin^2\phi\,\sigma_s^{\mathrm{OBK}} , \tag{14b}$$

$$\sigma_{p\pm1}^{\mathrm{PCI}} = \sigma_{p\pm1}^{\mathrm{OBK}} , \tag{14c}$$

$$\sigma_{sp,L}^{\mathrm{PCI}} = \cos^2\phi\,\sigma_{sp,L}^{\mathrm{OBK}} + \sin^2\phi\,(\sigma_{sp,L}^{\mathrm{OBK}})^* - i\sin\phi\cos\phi\,(\sigma_s^{\mathrm{OBK}} - \sigma_{p0}^{\mathrm{OBK}}) . \tag{14d}$$

The general expression of the OBK density matrix, entering Eq. (14), will be derived for arbitrary n in Appendix A. For the $n=2$ coherence matrix element we have found

$$\sigma_{sp,L}^{\mathrm{OBK}} = -i(16Z_T^5 Z_P^6\gamma\pi v_0^2/3v^2a_0^9D^{12})(1 - 3/7a_P^2D^2) , \tag{15}$$

with

$$\gamma = [\epsilon_T - \epsilon_P - (mv^2/2)]/\hbar v \tag{16}$$

and

$$D = [\gamma^2 + (1/na_P)^2]^{1/2} . \tag{17}$$

The OBK coherence matrix element is purely imaginary, which remains unaffected by the post-collision interaction, as can be seen from Eq. (14d). However, the sign depends on the velocity and the collision partners. For large v and $Z_P \approx Z_T$ we find $\mathrm{Im}\sigma_{sp,L}^{\mathrm{OBK}} > 0$ because of $\gamma < 0$. For a strongly asymmetric system ($Z_P \gg Z_T$), the second term in (15) can dominate even at considerably large v, leading to $\mathrm{Im}\sigma_{sp,L}^{\mathrm{OBK}} < 0$.

After normalization, the density matrix (13) contains two real and one complex independent parameters. For convenience, we choose, as the independent parameters, the relative angular momentum cross section

$$\frac{\sigma_{2p}}{\sigma_{2s}}=\frac{\sigma_{2p_0}+2\sigma_{2p_1}}{\sigma_{2s}}, \tag{18}$$

the alignment parameter

$$A=\frac{\sigma_{p0}-\sigma_{p1}}{\sigma_{p0}+\sigma_{p1}} \tag{19}$$

(which determines the anisotropy of the Lyα radiation), and the two relative coherence matrix elements

$$\frac{\mathrm{Re}(\sigma_{sp,L})}{\sigma_s}, \tag{20a}$$

$$\frac{\mathrm{Im}(\sigma_{sp,L})}{\sigma_s}. \tag{20b}$$

For the determination of the experimental Lyα polarization, the denominator in (19) must be replaced by $2.375\sigma_{p0}+3.749\sigma_{p1}$, which results[39] from averaging over several FS and HFS oscillation periods.

Figure 1 shows a comparison of the analytical approximation [Eq. (14)] with a full PCI calculation [Eq. (4)] including the splitting of the energy levels and the rotation of the internuclear axis. The excitation parameters [Eqs. (18)–(20)] are given as functions of R_0, the distance at which the PCI is switched on. The limit $R_0\to\infty$ corresponds to the OBK approximation. Evidently, the incorporation of the PCI leads to drastic changes for all parameters. For distances down to $R_0\approx\langle r\rangle_{n=2}$ (marked by an arrow), the agreement with the analytical model is surprisingly good and justifies the approximations leading to (14). A weak admixture of $\mathrm{Re}(\sigma_{sp,L})$ to the longitudinal s-p coherence in contrast to $\mathrm{Re}(\sigma_{sp,L})=0$ in the analytical approximation [Eq. (14)] arises from the energy splitting. For smaller distances $R_0<\langle r\rangle_{n=2}$ the rotation of the internuclear axis and the splitting become more important, resulting in larger discrepancies between the two treatments. Also, for smaller velocities the deviations would increase because of the larger dwell time in the target field. In the limit $R_0\ll\langle r\rangle_{2p}$, all density matrix elements become independent of R_0 because the splitting and the coupling tend to zero in the restricted space (4). The large degree of s-p coherence predicted by the PCI model corresponds to the preparation of a nearly pure state $\psi_{p0}+i\psi_s$ by the electron capture.

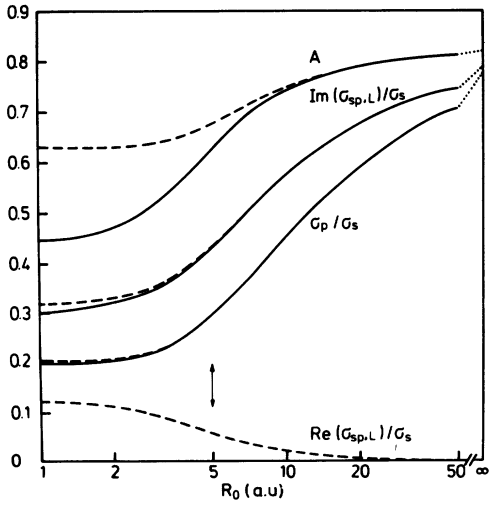

FIG. 1. Excitation parameters [Eqs. (18)–(20)] after electron capture $H^+ + H(1s) \to H(n=2) + H^+$ ($v = 2v_0$) as a function of the distance R_0, the starting point of the post-collisional evolution. —— Analytical approximation with $R_0 \approx Z_0$ [Eq. (14)]; --- full PCI calculation [Eq. (4)].

A. The relative l cross section

In Fig. 2 we show the relative l cross section σ_p/σ_s for the process $H^+ + H \to H(n=2) + H^+$ as a function of the velocity within several theoretical approximations. Unfortunately, except the data of Morgan *et al.*[41] at 26 keV, experimental data

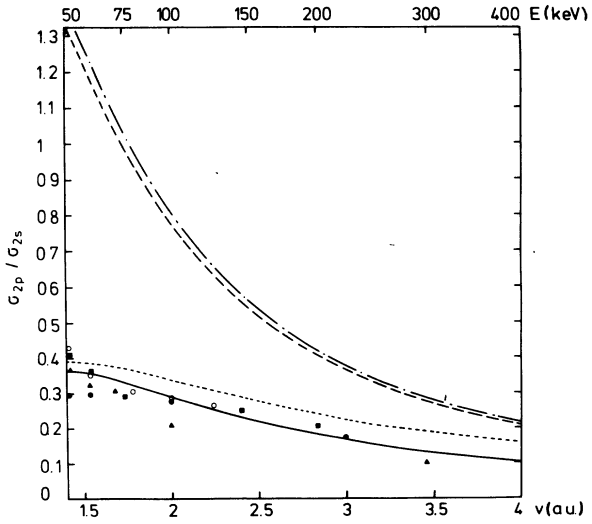

FIG. 2. Relative cross section σ_{2p}/σ_{2s} after electron capture $H^+ + H \to H(n=2) + H^+$ as a function of the impact velocity. —— Present PCI model [Eq. (14)]; --- OBK approximation; -·- Glauber phase approximation (Ref. 21); ··· CDW approximation (Ref. 42). Data from coupled-states calculations: ▲ Cheshire *et al.* (Ref. 33); ● Rapp *et al.* (Ref. 34); ■ Shakeshaft (Ref. 36); ○ Morrison and Öpik (Ref. 37).

are, to our knowledge, not available in the considered energy range. Therefore, the results of coupled-states calculations, with up to 35 states centered around the target and the projectile, may serve as the most reliable reference data. Obviously, the PCI approximation gives surprisingly good agreement with the coupled-states results. The differences in the angular momentum distribution between the PCI model and the Glauber approximation originate from the very different treatment of the electron-target interaction. The PCI model treats the interaction as a long-range coupling, while the Glauber approximation employs an electronic eikonal phase without coupling to intermediate states.

A discrepancy for the relative cross sections between the recent Glauber results of Eichler and Chan[21] given in Fig. 2 and those previously published by Dewangan[20] should be mentioned. The second-order CIS approximation, not shown in the Fig. 2, gives nearly the same relative l cross section as the OBK approximation.[29] The deviation of the CDW results[42] from the coupled-states calculation seems to be as large as for the PCI model. The success of our simple approximation demonstrates that the long-range coupling between degenerate projectile states is mainly responsible for the final relative l cross section in the coupled-states calculations. This is in accord with observations of Rapp *et al.*[34] and Winter and Lin[35] on the convergence of coupled-states calculations as a function of the number of the basis states.

For the reaction $H^+ + He(1s^2) \rightarrow H(n=2) + He^+$, a comparison is possible between the PCI results and the experimental data of Hughes *et al.*[5] for proton energies up to 120 keV (Fig. 3). In order to benefit from a one-electron description of the capture process, we approximate the initial He $1s$ state by a hydrogenic orbital with an effective charge[29] $Z_T = 1.35$ which reproduces the experimental binding energy. The strength of the PCI is determined by the asymptotic post-collision charge state $Z_T' = 1$, if inelastic two-electron processes are neglected. Except for its screening effect, the influence of the passive electron is neglected. Again, the use of the PCI brings the first-order treatment in accord with the data and the coupled-states calculation,[35] whereas first-order treatments without the long-range coupling (OBK or Glauber), and also the second-order CDW approximation,[43] show large discrepancies.

As Hughes *et al.*[5] have shown, the B1 approximation by Mapleton[44] for the reaction $H^+ + He(1s^2) \rightarrow H(n=3) + He^+$ also overestimates the relative cross section σ_{3p}/σ_{3s}. It might be expected that an application of the PCI model to the $n=3$ level would remove this difficulty.

B. Alignment

Kupfer and Winter have shown[45] that the effect of a strong electric surface field can explain the irregular velocity dependence of the alignment in hydrogen after electron capture in a beam-foil interaction. In our case of binary proton-atom collisions, the field of the target ion can play a similar role and can drastically change the alignment. For the reaction $H^+ + H(1s) \rightarrow H(n=2) + H^+$ we again take close-coupling calculations as reference data.[31,34,36,37] Even at high energies the PCI model (Fig. 4) reduces the OBK value for the

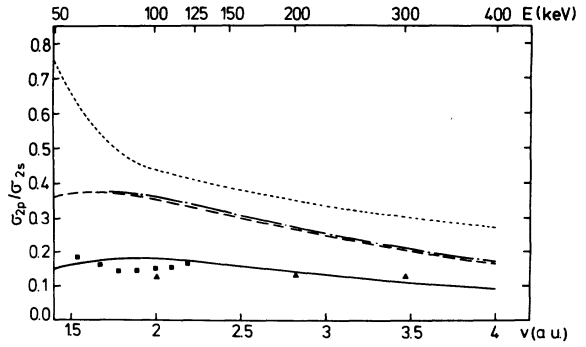

FIG. 3. Relative cross section σ_{2p}/σ_{2s} after electron capture $H^+ + He(1s^2) \rightarrow H(n=2) + He^+(?)$ as a function of the impact velocity. —— Present PCI model [Eq. (14)]; --- OBK approximation; -·-·- Glauber phase approximation with $Z_T = 1.687$ (Ref. 21); ··· CDW approximation (Ref. 43). Data: ■ experimental results of Hughes *et al.* (Ref. 5); ▲ coupled-states calculation of Winter and Lin (Ref. 35).

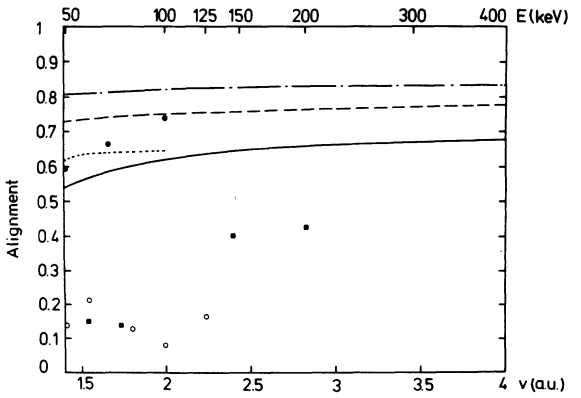

FIG. 4. Alignment parameter A after electron capture $H^+ + H(1s) \rightarrow H(n=2) + H^+$ as a function of the impact velocity. —— Present PCI model [Eq. (14)]; -·- OBK approximation; --- Glauber phase approximation of Dewangan [Eq. (20)]. Data from coupled-states calculations: ··· Gallaher and Wilets (Ref. 31); ● Rapp *et al.* (Ref. 34); ■ Shakeshaft (Ref. 36); ○ Morrison and Öpik (Ref. 37).

alignment A and improves the agreement with the coupled-states calculations. Nevertheless, the PCI values lie systematically too high compared with the most elaborate coupled-states calculations (Refs. 36 and 37). However, a definite statement about the accuracy can hardly be made because the spread of the different numerical results is large.

It should be noted that the A value in the Glauber approximation of Dewangan[20] differs at large velocities from the earlier calculations of Mittleman and Quong.[19] They have found an asymptotic value $A = 0.829$ in the limit $v \to \infty$, which lies close to the OBK value for all np states,

$$\lim_{v\to\infty} A = 0.846 . \tag{21}$$

The asymptotic results in B2 (Ref. 23) and the CDW approximation[29] are $A = -\frac{1}{5}$ and $A = -\frac{17}{25}$, respectively.

For the system $H^+ + He(1s^2) \to H(n=2) + He^+(?)$ there exist only a few polarization data of Teubner *et al.*[46] at lower velocities. In addition, they show remarkable disagreement with the angular-distribution measurements of Gaily *et al.*[47] below 15 keV. Nevertheless, we show in Fig. 5 the polarization data near v_0 after transformation to A [Eq. (19)], together with the PCI and the OBK approximation for $v > v_T$ (K-shell velocity). Again, notice the large difference between the two approximations. The PCI approximation shows a curvature similar to the experimental data, but shifted to higher velocities. The result must be handled with care because the theoretical uncertainties in the velocity range $v \approx v_0$ are large.

Comparison of the PCI model with the polarization data of Ellsworth *et al.*[48] for electron capture into highly stripped hydrogenic projectiles $O^{8+} + He(1s^2) \to O^{7+}(n=2) + He^+$ provides a preliminary test for the scaling properties for large Z_P. The primary OBK amplitude depends strongly on Z_P via momentum distribution and the energetic resonance defect. The PCI phase, on the other hand, is independent of the projectile charge [Eq. (12)]. For a highly asymmetric system $Z_P \gg Z_T$ we find quite a different field effect (Fig. 6). The alignment increases but the changes are relatively small in this case. The resulting curve lies near the single experimental point. Also shown are the alignment data of the Ly series emission after the electron capture $C^{6+} + He(1s^2) \to C^{5+}(np) + He^+$, which have been determined by the anisotropic angular distribution,[48] together with the $2p$ alignment in the OBK and PCI approximations. The agreement has only little significance because of the large hydrogenic transition probabilities ($\propto Z_P^4$), which may lead to considerable cascade contributions. The repopulation of the $2p$ state via cascade transitions would reduce the polarization.

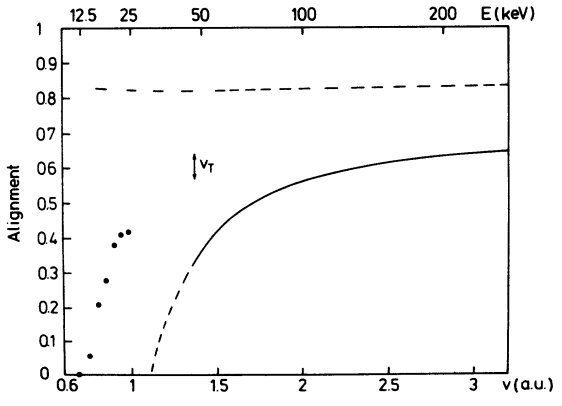

FIG. 5. Alignment parameter A after electron capture $H^+ + He(1s^2) \to H(n=2) + He^+(?)$ as a function of the impact velocity. —— Present PCI model [Eq. (14)]; --- OBK approximation; ● experimental data of Teubner *et al.* (Ref. 46).

IV. *s-p* COHERENCE

The s-p coherence may give an additional phase-sensitive test for the PCI model. Sellin *et al.*[13] have measured the longitudinal s-p coherence after the reaction $H^+ + He(1s^2) \to H(n=2) + He^+(?)$ at 186 keV. They used the fact that the time-resolved

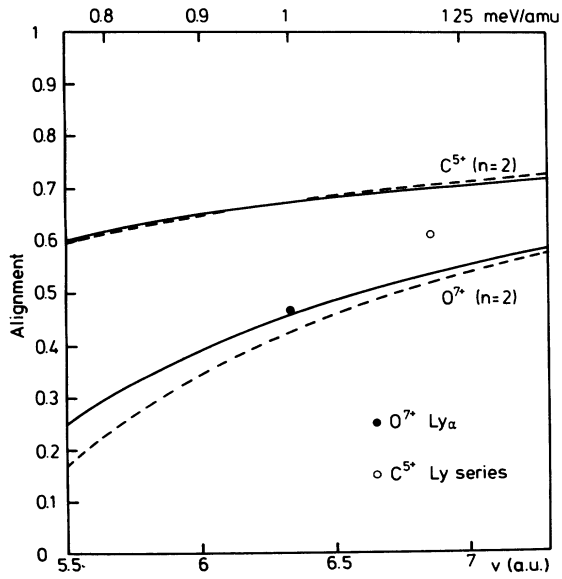

FIG. 6. Alignment parameter after electron capture $O^{8+} + He(1s^2) \to O^{7+}(n=2) + He^+(?)$ and $C^6 + He(1s^2) \to C^{5+}(2p) + He^+(?)$ as a function of the impact velocity. —— PCI model [Eq. (14)]; --- OBK approximation. Data: ● $O^{7+}(n=2)$ alignment, o averaged alignment of the angular distribution for the Ly series emission $\sum_n C^{5+}(np \to 1s)$ from Ellsworth *et al.* (Ref. 48).

Lyα intensity $I(+F_e,t)-I(-F_e,t)$ for emission in an external electric field parallel $(+F_e)$ and antiparallel $(-F_e)$ to the beam velocity, is directly proportional to the s-p coherence matrix element. An interpretation of the observed beat pattern requires both the collisionally prepared initial density matrix σ^{PCI} and the evolution operator U^{atomic}. The latter describes the atomic evolution under the combined influence of the internal interactions and the coupling to the external field. The second step was first attacked by Eck,[49] who used a two-state approximation involving the $s_{1/2}$ and $p_{1/2}$ states for low fields. On account of the experimental field strength $F_e = 525$ V/cm in Ref. 13, we shall derive a three-state approximation for the time-dependent Lyα signal, including also the $p_{3/2}$ state. The lifetime corrections and the HFS are approximately taken into account.

A. Homogeneous-field solution

An analytical treatment of the atomic evolution in an external field F_e,

$$\sigma(\pm F_e,t)=U^{\mathrm{atomic}}(\pm F_e,t)\sigma^{\mathrm{PCI}}U^{\mathrm{atomic}}(\pm F_e,t)^{*}\,, \quad (22)$$

is possible under the condition that the field is homogeneous, or equivalently time-independent in the reference system of the projectile. Neglecting for the moment the HFS, the Hamiltonian for the $m_j=\frac{1}{2}$ subspace of the $(p_{3/2},\ p_{1/2},\ s_{1/2})$ states is given by

$$H^{\pm}=\hbar\begin{pmatrix}\bar{\omega}_{\mathrm{FS}}-i\Gamma_p/2 & 0 & -\sqrt{2}\,V^{\pm}\\ 0 & -\omega_L/2-i\Gamma_p/2 & V^{\pm}\\ -\sqrt{2}\,V^{\pm} & V^{\pm} & \omega_L/2\end{pmatrix}. \quad (23)$$

In (23) ω_L denotes the Lamb shift frequency and $\bar{\omega}_{\mathrm{FS}}=\omega_{\mathrm{FS}}-\omega_L/2$, where ω_{FS} is the FS frequency. Γ_p is the zero-field decay constant of the $2p$ level. The interaction with the electric field is described by the coupling matrix element

$$V^{\pm}=\pm\frac{eF_e}{\hbar}\langle p_{1/2}|z|s_{1/2}\rangle=\pm\sqrt{3}\,a_p eF_e/\hbar\,. \quad (24)$$

The three-state approximation makes use of the fact that at medium field strength $(V_0=|V^{\pm}|\approx\omega_L)$, the $p_{1/2}$ and the $s_{1/2}$ states are strongly mixed, whereas the coupling to the $p_{3/2}$ state is relatively weak $(V_0/\omega_{\mathrm{FS}}\approx 0.1)$. Therefore, we first diagonalize the Hamiltonian in the $p_{1/2}-s_{1/2}$ subspace and perform, as a second step, a perturbational treatment of the coupling to the $p_{3/2}$ state in terms of the mixed $p_{1/2}-s_{1/2}$ states:

$$|2\rangle=\cos\theta\,|p_{1/2}\rangle-\sin\theta[1-i(\Gamma_p/2\omega)]\,|s_{1/2}\rangle\,, \quad (25a)$$

$$|3\rangle=\cos\theta\,|s_{1/2}\rangle+\sin\theta[1-i(\Gamma_p/2\omega)]\,|p_{1/2}\rangle\,, \quad (25b)$$

with

$$\omega=(\omega_L^2+4V_0^2)^{1/2}\,, \quad (26a)$$

$$\sin\theta\cos\theta=V^{\pm}/\omega\,. \quad (26b)$$

The evolution matrix can be approximated by

$$U^{\mathrm{atomic}}(\pm F_e,t)=Q(\pm F_e)\,\mathrm{diag}\big(\exp[-i(\omega_1-i\Gamma_p)t],\exp[-i(\omega_2-i\Gamma_2)t],\exp[-i(\omega_3-i\Gamma_3)t]\big)Q^{-1}(\pm F_e)\,, \quad (27)$$

where

$$\omega_1=\bar{\omega}_{\mathrm{FS}}+\sum_{i=2}^{3}\frac{\langle p_{3/2}|V^{\pm}|i\rangle\langle i|V^{\pm}|p_{3/2}\rangle}{\bar{\omega}_{\mathrm{FS}}-\bar{\omega}_i}\,, \quad (28a)$$

$$\omega_i=\bar{\omega}_i+\frac{\langle i|V^{\pm}|p_{3/2}\rangle\langle p_{3/2}|V^{\pm}|i\rangle}{\bar{\omega}_i-\bar{\omega}_{\mathrm{FS}}}\quad (i=2,3) \quad (28b)$$

$$\bar{\omega}_{2,3}=\mp\,\omega/2\,, \quad (28c)$$

$$\Gamma_{2,3}=\frac{\Gamma_p}{2}(1\pm\omega_L/\omega)\,. \quad (28d)$$

Note that due to the non-Hermitian damping part in (23), neither U nor Q are strictly unitary. On the present level of accuracy only first-order corrections in Γ_p must be retained because $\Gamma_p/\omega_L \approx 0.1$. Second-order lifetime corrections and terms of the order of $\Gamma_p/\omega_{\mathrm{FS}}$ can be neglected. The matrix $Q=\{|1\rangle,|2\rangle',|3\rangle'\}$ consists of the approximate eigenvectors

$$|1\rangle=|p_{3/2}\rangle+\sum_{i=2}^{3}|i\rangle\frac{\langle i|V^{\pm}|p_{3/2}\rangle}{\bar{\omega}_{\mathrm{FS}}-\bar{\omega}_i}\,, \quad (29a)$$

$$|i\rangle'=|i\rangle+|p_{3/2}\rangle\frac{\langle p_{3/2}|V^{\pm}|i\rangle}{\bar{\omega}_i-\bar{\omega}_{\mathrm{FS}}}\quad (i=2,3) \quad (29b)$$

expressed in components of the FS basis. We have tested the accuracy of the approximation (27) by a numerical solution of the eigenvalue problem for (23). We have found changes of only a few percent even for a medium field strength $V_0\approx\omega_L$. The field-modified Lamb beat frequency $\omega_{32}=\omega_3-\omega_2$ agrees with the numerical value to within 1%. Only for the small field-induced damping constant Γ_3 a larger discrepancy of about 20% occurs, which influences the beat pattern only slightly.

For time-resolved quantum beat signals the hyperfine structure of the $n=2$ level must also be included, although the splitting is small $(\Delta\omega^{\mathrm{HFS}}/$

$\omega_L \lesssim \frac{1}{5}$). For the 16 HFS states of the $n=2$ manifold a similar approximate treatment for the evolution in an external field is possible. The final, rather involved, expressions for the coherent signal, $I(+F_e,t)-I(-F_e,t)$, which is directly proportional to the coherence matrix element and the incoherent signal, $I(+F_e,t)+I(-F_e,t)$, and depend only on the cross sections, are given in the Appendix B. As a check, we have applied Eq. (B3) to the beam-foil data of Gaupp and Andrä,[50] assuming a pure $s_{1/2}$ initial state for times $t \gg \Gamma_p^{-1}$, and find good agreement for the low-frequency modulation of the Lamb beat amplitude resulting from the HFS.

The ion-atom collision data of Sellin *et al.*[13] (Fig. 7) show in the coherent signal a phase delay with respect to a negative-going sine oscillation if one chooses the center of the gas cell as the origin. This was explained by a delayed switch-on of the electric field in the gas-cell region. Furthermore an upward shift of the coherent signal could be observed, which was interpreted as a stray-light effect. Using the PCI density matrix [Eq. (14)] and a simplified homogeneous-field solution of (22), we have found in the previous treatment[38] reasonable agreement with the data after subtracting the observed shift and adjusting the time origin in accordance with the suggestions of Sellin *et al.*[13]

B. Inhomogeneous-field solution

A more detailed inspection of the analytical expression (B2) shows that at the experimental field strength ($F_e = 525$ V/cm) the amplitudes of the leading shift and cosine beat terms, which are both proportional to $\mathrm{Re}\sigma_{sp,L}$, have a different sign. Thus, Eq. (B2), as it stands, cannot describe the observed beat pattern. This difficulty cannot be removed by any other choice of the initial density matrix elements and gives a hint to an additional influence of the experimental setup not covered by the intensity formula (B2). In order to avoid the *ad hoc* corrections mentioned above, we now take into account the spatial inhomogeneity of the electric field in the gas-cell region due to the apertures in the condenser plates. For the sake of simplicity we choose the following form for the switch on of the field averaged over the beam diameter:

$$F_e(Z) = F_e(1+e^{-(Z-\Delta s/2)/w})^{-1} . \tag{30}$$

The electric field reaches half of its asymptotic value, F_e, at the exit plane of the gas cell ($Z = \Delta s/2$, gas-cell length $\Delta s = 0.05$ cm). Changing the width w of the transition region from 0.02 to 0.04 cm, no drastic effect on the beat pattern was found. With (30) the Hamiltonian (23) becomes explicitly time dependent in the projectile frame ($Z = vt$). The constant-field solution [Eqs. (B2) and (B3)] must then replaced by a numerical calculation of the evolution of the initial-density matrix [Eq. (22)]. Owing to the field inhomogeneity, the resulting density matrix contains an average over all capture positions in the target gas cell

$$\sigma(\pm F_e,t) = \frac{v}{\Delta s}\int_{-\Delta s/2v}^{\Delta s/2v} dt_0 U^{\mathrm{atomic}}(\pm F_e,t,t_0) \times \sigma^{\mathrm{PCI}} U^{\mathrm{atomic}}(\pm F_e,t,t_0)^* . \tag{31}$$

The integration attenuates the fine structure beats completely, whereas the field-modified Lamb beats, slightly modified by the HFS, survive. The influence of cascade contributions, which may be possible for larger times, are neglected.

The theoretical time-resolved intensities are shown in Fig. 7 for two different values of the beat attenuation factor B. Beat averaging due to the finite detection window, as well as an effective target length larger than the cell extension, is taken into account. The interesting result is that the transient-field behavior (30) leads to both the delayed beat phase and the shift of the coherent signal, as experimentally observed. The occurrence of the shift can be traced back to the effect of the zero-field Hamiltonian on the density matrix in the transition region.

The agreement between experimental and calculated beat phase confirms the PCI result for the s-p coherence phase ($\mathrm{Im}\sigma_{sp,L} > 0$, $\mathrm{Re}\sigma_{sp,L} = 0$). However, the cosine term proportional to $\mathrm{Re}\sigma_{sp,L}$

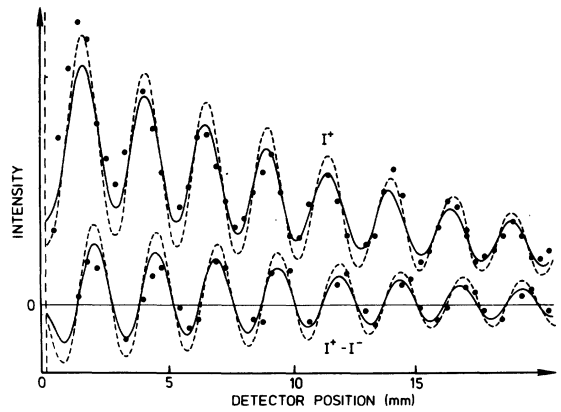

FIG. 7. Lyα intensity versus distance downstream from the He gas cell at field strength 525 V/cm and proton velocity $v = 2.73v_0$ ($w = 0.04$ cm). I^+, calculated intensity for electric field parallel to the beam; $I^+ - I^-$, signal difference between fields parallel and antiparallel to the beam [Eq. (B2)]. —— Beat attenuation factor $B = 0.56$; --- $B = 0.8$; experimental data from Sellin *et al.* (Ref. 13).

in the coherence signal [Eq. (B2)] is partially suppressed compared with the sine-dependent term proportional to $\mathrm{Im}\sigma_{sp,L}$. Therefore, the accuracy of the phase determination should not be overestimated and the presence of a small $\mathrm{Re}\sigma_{sp,L}$ contribution cannot be ruled out. Interestingly enough, we find a better fit for both the intensities $I(+F_e)$ and $I(+F_e)-I(-F_e)$ if we choose $B=0.56$ for the beat attenuation instead of the experimental value $B\approx 0.8$. The origin of this discrepancy is not yet clear. However, an independent check is possible for the modulation depth of $I(+F_e)$ which is roughly given by that of the incoherent signal. The latter is essentially determined by the relative cross section σ_p/σ_s. The agreement of the PCI density matrix elements with the data of Hughes *et al.*[5] at lower velocities (Fig. 3) supports the theoretical modulation depth. Larger average effects of the experimental setup than previously estimated may be a possible source for this discrepancy. In the immediate vicinity of the exit plane of the gas cell, marked by the broken line, one can observe deviations of the theoretical curve from the periodic structure, which reflect the inhomogeneity of the field. The experimental signal $I(+F_e)$ exceeds the theoretical curve during the first beat periods. This may be caused by stray-light effects of target rest-gas excitation behind the cell. As observed by Hughes *et al.*,[5] the $He^+(n=4\rightarrow n=2)$ transition can significantly contribute to the photon production in the Lyα region after $[H^+ + He(1s^2)]$ collisions in the considered energy range. Thus, considering the uncertainties discussed above, the overall agreement of the calculated s-p coherence with the data is quite satisfactory.

V. CONCLUSIONS

We have shown that drastic changes in the hydrogenic excited state density matrix after electron capture occur if the post-collisional Stark effect due to target-ion field interaction is incorporated. This is in accordance with similar results for direct excitation.[51] The present approach can improve the OBK approximation at medium-to-high energies within a simple analytical treatment. It is confirmed by reasonable agreement with various experimental data for all parameters of the $n=2$ density matrix. This agreement only holds for the relative density matrix elements, but not for the absolute substate cross sections. The PCI model can also be applied to refined first- and second-order treatments leading to better absolute sublevel cross sections.

Removal of the axial symmetry could give still more information on the collision process. Investigation of the coherences between magnetic substates in a nonaxially symmetric scattering process with angle selection is in progress.

ACKNOWLEDGMENTS

I wish to thank Professor Gabriel, Dr. Kupfer, Dr. Schröder, Professor Andrä, and Dr. Astner for helpful suggestions and discussions. I am also grateful to Dr. Winscom for a critical reading of the manuscript. This work is part of the research program of the Sonderforschungsbereich 161, supported by the Deutsche Forschungsgemeinshaft.

APPENDIX A: THE OBK DENSITY MATRIX

The density matrix (13) for an arbitrary final state n in the OBK approximation can be calculated in closed form. The diagonal elements for l subshells with $n\leq 3$ were first given by Omidvar.[52] After substituting explicit expressions[53] of the amplitude (2) into (13) we find by integrating over the impact parameter

$$\sigma^n_{l|m|,l'|m'|}=\pi\delta_{m,m'}i^{l-l'}\sum_{t,t'=0}^{n-l-1}\sum_{j,j'=0}^{l-|m|}\sum_{s,s'=0}^{(l-|m|-j)/2}C^{nlm}_{tjs}C^{nl'm}_{t'j's'}\frac{(l+l'+t+t'-s-s'-|m|+4)!\gamma^{j+j'}}{(l+l'+t+t'-s-s'+5)!}\times D^{-10-2(l+l'+t+t'-s-s'-|m|)}, \tag{A1}$$

with

$$C^{nlm}_{tjs}=(-1)^{(l-|m|-j)/2+t-s}\cos\left(\frac{\pi}{2}(m+|m|)\right)\cos\left(\frac{\pi}{2}(l-|m|-j)\right)\times\left(\frac{v_0}{v}\right)\left(\frac{(l-|m|)!(n-l-1)!Z_T^5Z_P^{5+2l}}{(2l+1)(l+|m|)!(n+l)!a_0^{8+2l}}\right)^{1/2}\frac{2^{4+l}l!(n+l+t)!}{n^{l+2}(2l)!(n-l-t-1)!}\times\frac{\Gamma(l+\frac{3}{2})(l+|m|+j)!(na_p)^{2s-2t+j+|m|-l}}{\Gamma(l+t+\frac{3}{2})t!j!s!\left(\frac{l+|m|+j}{2}\right)!\left(\frac{l-|m|-j}{2}-s\right)!}. \tag{A2}$$

APPENDIX B: THE Lyα INTENSITY IN THE ELECTRIC FIELD

For low-to-medium field strength ($V_0 \lesssim \omega_L$) an approximate expression for the time-resolved Lyα intensity can be derived. For a usual 90° detection geometry and an average over the unresolved fine structure the intensity reads in terms of the HFS density matrix elements

$$\begin{aligned} I(t) = I_0\big(&\tfrac{3}{8}\langle p_{3/2}, 22|\sigma(t)|p_{3/2}, 22\rangle + \tfrac{9}{16}\langle p_{3/2}, 21|\sigma(t)|p_{3/2}, 21\rangle + \tfrac{5}{16}\langle p_{3/2}, 20|\sigma(t)|p_{3/2}, 20\rangle + \tfrac{7}{16}\langle p_{3/2}, 11|\sigma(t)|p_{3/2}, 11\rangle \\ &+\tfrac{5}{16}\langle p_{3/2}, 10|\sigma(t)|p_{3/2}, 10\rangle - (\sqrt{3}/8)\,\mathrm{Re}\langle p_{3/2}, 11|\sigma(t)|p_{3/2}, 21\rangle + \tfrac{1}{4}\langle p_{1/2}, 00|\sigma(t)|p_{1/2}, 00\rangle + \tfrac{1}{4}\langle p_{1/2}, 10|\sigma(t)|p_{1/2}, 10\rangle \\ &+\tfrac{1}{2}\langle p_{1/2}, 11|\sigma(t)|p_{1/2}, 11\rangle - (1/4\sqrt{2})\,\mathrm{Re}[\langle p_{1/2}, 10|\sigma(t)|p_{3/2}, 10\rangle - \langle p_{1/2}, 11|\sigma(t)|p_{3/2}, 11\rangle + \langle p_{1/2}, 00|\sigma(t)|p_{3/2}, 20\rangle \\ &+\sqrt{3}\langle p_{1/2}, 11|\sigma(t)|p_{3/2}, 21\rangle]\big), \end{aligned} \tag{B1}$$

where the states are labeled by $|l_j FM_F\rangle$. In (B1) we have exploited the axial symmetry of the density matrix which remains preserved during the evolution in a field (anti) parallel to the beam. The 16×16 energy matrix of the $n=2$ level factorizes into two (3×3) blocks for $M_F = 0, 2$ (4×4) blocks for $M_F = \pm 1$ and two (1×1) blocks for $M_F = \pm 2$. The analytical approximation is based on the observation that each of the nontrivial blocks contain a strongly coupled (2×2) subspace originating from the $p_{1/2}$ and $s_{1/2}$ state and a weak coupling to one or two $p_{3/2}$ states. Consequently, the perturbational treatment, sketched in Sec. IV, is also applicable to the hyperfine structure. Within the perturbational treatment, the first-order corrections due to the $p_{3/2}$ coupling ($\sim V_0/\omega_{FS}$), the linewidth ($\sim\Gamma_p/\omega_L$), or the HFS ($\sim\Delta\omega^{HFS}/\omega_L$) are included. The intensity formula can be simplified by retaining only beat terms with frequencies $\lesssim\omega_L$ because the FS beats are not resolved. After a tedious but straightforward calculation we find for the coherent part of the signal [for notation, see Eqs. (24)–(29)]:

$$\begin{aligned} I(+F_\theta, t) - I(-F_\theta, t) = 2I_0\Big(&\mathrm{Re}\langle s_{1/2}, \tfrac{1}{2}|\sigma^{PCI}|p_{1/2}, \tfrac{1}{2}\rangle \\ &\times\Big\{e^{-\Gamma}P^t V_0\Big(\frac{\cos^2\theta}{\bar\omega_{FS}-\omega/2}+\frac{\sin^2\theta}{\bar\omega_{FS}+\omega/2}\Big)\big[\tfrac{37}{8}+\tfrac{3}{8}\cos(\omega_{\Delta F}t)\big] \\ &-2\sin\theta\cos\theta\Big[e^{-\Gamma_2 t}\Big(\cos^2\theta+V_0\frac{3\sin\theta\cos\theta}{\bar\omega_{FS}+\omega/2}\Big)-e^{-\Gamma_3 t}\Big(\sin^2\theta-V_0\frac{3\sin\theta\cos\theta}{\bar\omega_{FS}-\omega/2}\Big) \\ &-e^{-\Gamma t}\Big(\cos 2\theta\, c(t)+(1-2\cos^2 2\theta)\delta c(t)-\cos 2\theta\frac{\Gamma_p}{\omega}\vartheta(t)\Big)\Big] \\ &+e^{-\Gamma t}V_0 c(t)\Big[5\sin^2\theta\cos^2\theta\Big(\frac{1}{\bar\omega_{FS}+\omega/2}+\frac{1}{\bar\omega_{FS}-\omega/2}\Big)-\frac{\sin^4\theta}{\bar\omega_{FS}+\omega/2}-\frac{\cos^4\theta}{\bar\omega_{FS}-\omega/2}\Big]\Big\} \\ &+\mathrm{Im}\langle s_{1/2}, \tfrac{1}{2}|\sigma^{PCI}|p_{1/2}, \tfrac{1}{2}\rangle\Big\{2\sin\theta\cos\theta\Big[e^{-\Gamma t}\Big(\vartheta(t)+\frac{\Gamma_p}{\omega}c(t)-\cos 2\theta\delta\vartheta(t)\Big) \\ &-\frac{\cos^2\theta\Gamma_p}{\omega}e^{-\Gamma_2 t}-\sin^2\theta\frac{\Gamma_p}{\omega}e^{-\Gamma_3 t}\Big] \\ &+V_0\vartheta(t)e^{-\Gamma t}\Big(\frac{\sin^4\theta}{\bar\omega_{FS}+\omega/2}-\frac{\cos^4\theta}{\bar\omega_{FS}-\omega/2}\Big)\Big\}\Big) \end{aligned} \tag{B2}$$

and for the incoherent part

$$\begin{aligned} I(+F_\theta, t) + I(-F_\theta, t) = 2I_0\Big(&\langle p_{3/2}, \tfrac{3}{2}|\sigma^{PCI}|p_{3/2}, \tfrac{3}{2}\rangle\big[\tfrac{27}{32}-\tfrac{3}{32}\cos(\omega_{\Delta F}t)\big]e^{-\Gamma_p t} \\ &+\langle p_{3/2}, \tfrac{1}{2}|\sigma^{PCI}|p_{3/2}, \tfrac{1}{2}\rangle\big[\tfrac{37}{32}+\tfrac{3}{32}\cos(\omega_{\Delta F}t)\big]e^{-\Gamma_p t}+\langle p_{1/2}, \tfrac{1}{2}|\sigma^{PCI}|p_{1/2}, \tfrac{1}{2}\rangle \\ &\times\Big\{e^{-\Gamma_2 t}\Big(\cos^4\theta+V_0\frac{\cos^3\theta\sin\theta}{\bar\omega_{FS}+\omega/2}\Big)+e^{-\Gamma_3 t}\Big(\sin^4\theta-V_0\frac{\cos\theta\sin^3\theta}{\bar\omega_{FS}-\omega/2}\Big) \\ &+2e^{-\Gamma t}\sin^2\theta\cos^2\theta\Big[c(t)-2\cos 2\theta\delta c(t)-\frac{2\Gamma_p}{\omega}\vartheta(t)-\frac{\omega}{2}c(t)\Big(\frac{\cos^2\theta}{\bar\omega_{FS}-\omega/2}-\frac{\sin^2\theta}{\bar\omega_{FS}+\omega/2}\Big)\Big]\Big\} \\ &+\sin^2\theta\cos^2\theta\langle s_{1/2}, \tfrac{1}{2}|\sigma^{PCI}|s_{1/2}, \tfrac{1}{2}\rangle \\ &\times\Big\{e^{-\Gamma_2 t}\Big(1+V_0\frac{\tan\theta}{\bar\omega_{FS}+\omega/2}\Big)+e^{-\Gamma_3 t}\Big(1-V_0\frac{\cot\theta}{\bar\omega_{FS}-\omega/2}\Big) \\ &-2e^{-\Gamma t}\Big[c(t)-2\cos 2\theta\delta c(t)-\frac{\omega}{2}c(t)\Big(\frac{\cos^2\theta}{\bar\omega_{FS}-\omega/2}-\frac{\sin^2\theta}{\bar\omega_{FS}+\omega/2}\Big)\Big]\Big\} \\ &+2\sqrt{2}\,\mathrm{Re}\langle p_{1/2}, \tfrac{1}{2}|\sigma^{PCI}|p_{3/2}, \tfrac{1}{2}\rangle\sin^2\theta\cos^2\theta\omega \\ &\times\Big[\frac{\sin^2\theta}{\bar\omega_{FS}-\omega/2}e^{-\Gamma_3 t}-\frac{\cos^2\theta e^{-\Gamma_2 t}}{\bar\omega_{FS}+\omega/2}+e^{-\Gamma t}c(t)\Big(\frac{\cos^2\theta}{\bar\omega_{FS}-\omega/2}-\frac{\sin^2\theta}{\bar\omega_{FS}+\omega/2}\Big)\Big]\Big) \end{aligned} \tag{B3}$$

as a function of the initial density matrix elements in the FS basis. For a spin-independent capture process these are related to the orbital-angular-momentum density matrix by

$$\langle l_j m_j | \sigma^{\mathrm{PCI}} | l_j', m_j' \rangle = \tfrac{1}{2} \sum_{\substack{m_l m_l' \\ m_s}} \langle l_j m_j | l m_l s m_s \rangle \langle l' m_l', s m_s | l_j', m_j' \rangle \langle l m_l | \sigma^{\mathrm{PCI}} | l' m_l' \rangle . \tag{B4}$$

In (B2) and (B3) $\omega_{\Delta F}$ denotes the field-modified HFS beat frequency

$$\omega_{\Delta F} = \omega_{F=2} - \omega_{F=1} + V_0^2 \left(\frac{\cos^2\theta}{\bar{\omega}_{\mathrm{FS}} - \omega/2} + \frac{\sin^2\theta}{\bar{\omega}_{\mathrm{FS}} + \omega/2} \right) \tag{B5}$$

and the HFS-modulated Lamb beat functions are given by

$$c(t) = \tfrac{1}{4}(\cos\omega_\alpha t + \cos\omega_\beta t + 2\cos\omega_\gamma t), \tag{B6a}$$

$$s(t) = \tfrac{1}{4}(\sin\omega_\alpha t + \sin\omega_\beta t + 2\sin\omega_\gamma t). \tag{B6b}$$

The frequencies in (B6) are denoted by

$$\omega_k = [(\omega_L + \Delta\omega_k^{\mathrm{HFS}})^2 + 4V_0^2]^{1/2} - 2V_0^2 \left(\frac{\cos^2\theta}{\bar{\omega}_{\mathrm{FS}} - \omega/2} - \frac{\sin^2\theta}{\bar{\omega}_{\mathrm{FS}} + \omega/2} \right), \tag{B7}$$

where $\Delta\omega_k^{\mathrm{HFS}}$ ($k = \alpha, \beta, \gamma$) are the HFS splittings of the $p_{1/2}$ and $s_{1/2}$ states in the two (3×3) blocks ($k = \alpha, \beta$) and the (4×4) block ($k = \gamma$). In the limit $\Delta\omega_k^{\mathrm{HFS}} \to 0$, (B6) reduces to

$$c(t) = \cos\omega_{32} t, \tag{B8a}$$

$$s(t) = \sin\omega_{32} t. \tag{B8b}$$

The first-order corrections in the beat amplitudes are proportional to

$$\delta c(t) = \tfrac{1}{4}(\delta\omega_\alpha \cos\omega_\alpha t + \delta\omega_\beta \cos\omega_\beta t + 2\delta\omega_\gamma \cos\omega_\gamma t), \tag{B9a}$$

$$\delta s(t) = \tfrac{1}{4}(\delta\omega_\alpha \sin\omega_\alpha t + \delta\omega_\beta \sin\omega_\beta t + 2\delta\omega_\gamma \sin\omega_\gamma t), \tag{B9b}$$

with

$$\delta\omega_k = \Delta\omega_k^{\mathrm{HFS}}/\omega . \tag{B10}$$

For the nonbeating parts first-order corrections vanish. As can be seen from (B7) and (B10), the HFS corrections decrease with increasing field strength which corresponds to the decoupling of the hyperfine states by the external field.

[1] R. F. Stebbings, R. A. Young, C. L. Oxley, and H. Ehrhardt, Phys. Rev. 138, A1312 (1965).
[2] G. Ryding, A. B. Wittkower, and H. B. Gilbody, Proc. Phys. Soc. London 89, 547 (1966).
[3] J. E. Bayfield, Phys. Rev. Lett. 20, 1223 (1968).
[4] T. Gaily, Phys. Rev. 178, 207 (1969).
[5] R. H. Hughes, E. D. Stokes, Song-Sik Choe, and T. J. King, Phys. Rev. A 4, 1453 (1971); R. H. Hughes, C. Stigers, B. Doughty, and D. Stokes, Phys. Rev. A 1, 1424 (1970).
[6] E. P. Andreev, V. A. Ankudinov, and S. V. Bobashev, Zh. Eksp. Teor. Fiz. 50, 565 (1966) [Sov. Phys.—JETP 23, 375 (1966)].
[7] H. F. Helbig and E. Everhart, Phys. Rev. 136, A674 (1964).
[8] C. L. Cocke, R. J. MacDonald, B. Curnutte, S. L. Varghese, and R. Randall, Phys. Rev. Lett. 36, 782 (1976).
[9] T. R. Bratton, C. L. Cocke, and J. R. MacDonald, J. Phys. B 10, L517 (1977).
[10] F. J. Eriksen, D. H. Jaecks, W. de Rijk, and J. Macek, Phys. Rev. A 14, 119 (1976).
[11] W. Wittmann and H. J. Andrä, Z. Phys. A 288, 335 (1978).
[12] R. Hippler, H. Kleinpoppen, and H. O. Lutz, in *Proceedings of the 11th International Conference on the Physics of Electronic and Atomic Collisions, Kyoto, 1979*, edited by K. Takayangi and N. Oda (North-Holland, Amsterdam, 1980), p. 611.
[13] I. A. Sellin, L. Liljeby, S. Mannervik, and S. Hultberg, Phys. Rev. Lett. 42, 570 (1979); L. Liljeby, S. Mannervik, S. Hultberg, and I. A. Sellin, Z. Phys. A 288, 321 (1978).
[14] J. C. Dehaes and W. Singer, Phys. Lett. 75A, 276 (1980).
[15] H. C. Brinkmann and H. A. Kramers, Proc. R. Soc. Amsterdam 33, 973 (1930).
[16] D. R. Bates and A. Dalgarno, Proc. Phys. Soc. London A65, 919 (1952).
[17] J. D. Jackson and H. Schiff, Phys. Rev. 89, 359 (1953).
[18] D. R. Bates and R. McCaroll, Adv. Phys. 11, 39 (1962).
[19] M. Mittleman and J. Quong, Phys. Rev. 167, 74 (1969).

[20]D. P. Dewangan, J. Phys. B 8, L119 (1975); 10, 1083 (1977).
[21]J. Eichler and F. T. Chan, Phys. Rev. A 20, 104 (1979); F. T. Chan and J. Eichler, *ibid.* 20, 1841 (1979).
[22]P. J. Kramer, Phys. Rev. A 6, 2125 (1972).
[23]J. S. Briggs and L. Dubé, J. Phys. B 13, 771 (1980).
[24]D. H. Jakubassa-Amundsen and P. A. Amundsen, Z. Phys. A 297, 203 (1980).
[25]I. M. Cheshire, Proc. Phys. Soc. London 84, 89 (1964).
[26]D. Belkic, J. Phys. B 10, 3491 (1977).
[27]V. S. Nikolaev, Zh. Eksp. Teor. Fiz. 51, 1263 (1966) [Sov. Phys.—JETP 24, 847 (1967)].
[28]M. R. C. McDowell and J. P. Coleman, *Introduction to the Theory of Ion-Atom Collisions* (North-Holland, Amsterdam, 1970), p. 384.
[29]D. Belkic, R. Gayet, and A. Salin, Phys. Rep. 56, 279 (1979).
[30]D. F. Gallaher and L. Wilets, Phys. Rev. 147, 13 (1966).
[31]L. Wilets and D. F. Gallaher, Phys. Rev. 169, 139 (1968).
[32]L. T. Sin Fai Lam, Proc. Phys. Soc. London 92, 67 (1967).
[33]I. M. Cheshire, D. F. Gallaher, and A. J. Taylor, J. Phys. B 3, 813 (1970); I. M. Cheshire, *ibid.* 1, 428 (1968).
[34]D. Rapp and D. Dinwiddie, J. Chem. Phys. 57, 4919 (1972); D. Rapp, D. Dinwiddie, and D. Storm, Phys. Rev. A 5, 1290 (1972).
[35]T. G. Winter and C. C. Lin, Phys. Rev. A 10, 2141 (1974).
[36]R. Shakeshaft, J. Phys. B 8, 1114 (1975); Phys. Rev. A 18, 1930 (1978).
[37]H. G. Morrison and U. Opik, J. Phys. B 11, 473 (1978); 12, L685 (1979).
[38]J. Burgdörfer, Phys. Rev. Lett. 43, 505 (1979).
[39]I. C. Percival and M. J. Seaton, Philos. Trans. R. Soc. London A251, 113 (1958); U. Fano and J. Macek, Rev. Mod. Phys. 45, 553 (1973).
[40]R. Shakeshaft and L. Spruch, Rev. Mod. Phys. 51, 369 (1979).
[41]T. J. Morgan, J. Geddes, and H. B. Gilbody, J. Phys. B 6, 2118 (1973).
[42]D. Belkic and R. Gayet, J. Phys. B 10, 1911 (1977).
[43]D. Belkic and R. Gayet, J. Phys. B 10, 1923 (1977).
[44]R. A. Mapleton, Phys. Rev. 122, 528 (1961).
[45]E. Kupfer and H. Winter, Z. Phys. A 285, 3 (1978).
[46]P. Teubner, W. Kauppila, W. Fite, and R. Girnius, Phys. Rev. A 2, 1763 (1970).
[47]T. Gaily, D. H. Jaecks, and R. Geballe, Phys. Rev. 167, 81 (1968).
[48]L. D. Ellsworth, B. L. Doyle, and U. Schiebel, Phys. Rev. A 19, 943 (1979); L. D. Ellsworth, J. A. Guffey, E. Salzborn, and J. R. MacDonald, Phys. Rev. A 17, 1438 (1977).
[49]T. G. Eck, Phys. Rev. Lett. 31, 270 (1973).
[50]A. Gaupp, diploma thesis, Freie Universitat Berlin (unpublished); H. J. Andrä, Phys. Scr. 9, 257 (1974).
[51]Y. Band, J. Phys. B 13, 3215 (1980).
[52]K. Omidvar, Phys. Rev. 153, 121 (1967).
[53]J. Burgdörfer, J. Phys. B 14, 1019 (1981).